

Finite Element Analysis Of Different Spinal Cage Designs For Posterior Lumbar Interbody Fusion

Kugendran A/L Mahendran
College of Engineering, Universiti Malaysia Pahang

Muhammad Hilmi bin Jalil
Faculty of Mechanical and Automotive Engineering Technology, Universiti Malaysia Pahang

<https://doi.org/10.5109/4738560>

出版情報 : Proceedings of International Exchange and Innovation Conference on Engineering & Sciences (IEICES). 7, pp.51-57, 2021-10-21. Interdisciplinary Graduate School of Engineering Sciences, Kyushu University

バージョン :

権利関係 :



Finite Element Analysis Of Different Spinal Cage Designs For Posterior Lumbar Interbody Fusion

Kugendran A/L Mahendran¹, Muhammad Hilmi bin Jalil^{2*}

¹College of Engineering, Universiti Malaysia Pahang, 26600 Pekan, Pahang,

²Faculty of Mechanical and Automotive Engineering Technology, Universiti Malaysia Pahang, 26600, Pekan, Pahang.

*Corresponding author email: muhammadhilmi@ump.edu.my

Abstract: *The study on spinal cage designs for their implementation in the medical field is developing over the years. Currently, many designs have been studied varying from the biomaterials and the designs. This study aimed to determine the best design structure of an annealed titanium spinal cage with the integration of porous holes and to attain its mechanical performance under different loadings before topology optimization. 8 specimens were designed and analyzed based on porosity percentage, MIT, and FEA before undergoing topology optimization. The analysis was conducted on two loadings applied simultaneously to resemble the human body weight and the motion of the lumbar column. Results showed that the stress concentration of all specimens increased accordingly as the porosity volume increases, thus specimen 2 was selected due to it having the second-lowest stress concentration but also the more adequate pore volume for the bone graft filling.*

Keywords: PLIF, Lumbar Cage, Stress Analysis, Topology Optimization

1. INTRODUCTION

Lumbar or spinal cage fusion is a method of treatment that is required to treat a specific disease called disc spondylosis or degenerative disc disease. Methods of surgery include the Posterior Lumbar Interbody Fusion (PLIF), Anterior Lumbar Interbody Fusion (ALIF), Transforaminal Lumbar Interbody Fusion (TLIF), etc. Disc spondylosis refers to the degeneration of an intervertebral disc that sits between two adjacent vertebrae, thus an external implant is required to be fused into the lumbar column for the fixation of the vertebrae. The spinal cage has to serve its purpose in terms of an implant replacement of the actual intervertebral disc, as well as being able to serve its purpose of a connecting medium between two vertebrae. Various designs of lumbar cages are being applied in the medical field up till today yet it has still been improvised as the technology and resources develop.

The two main factors that give an immediate effect to the biomechanical performance of the spinal cages are the biomaterials and the spinal cage designs. PLIF spinal cages are mostly manufactured using Polyetheretherketone (PEEK) and titanium alloy [1]. Each material undoubtedly has its unique material properties that would give different outputs of stress and strain analysis. Despite PEEK having its term of being used as the most common material, titanium alloy is rather more favourable in terms of clinical outputs such as the cage subsidence, and the complication rates mostly yield towards titanium.

On the other hand, cage designs have always been a confusion in the current industry. Several criteria are commonly found among the commercialized designs such as the cylindrical, threaded, biconvex and biconcave designs as well as porosity integrated cages[2]. Porous holes are required to be implemented in the spinal cages. It serves the significant purpose of being a medium for the filling of bone graft material, which helps to aid the fusion rate and allowing the transport of fluid into the cages. However, only limited studies showed that with the alteration of porosity volume, the performance of the cages is affected[3].

Therefore, this study was conducted to analyze the designs of spinal cages in terms of porosity volume and their stress analysis that includes Von Misses Stress and

Maximum Principal Stress, using Finite Element Analysis under two loading conditions, force and moment. Then, using the topology optimization, comparison are to be made. The material used in this study was annealed titanium alloy and the pore volumes were varied in terms of holes and slots integration on 8 different cages including the control study.

2. MATERIALS AND METHOD

2.1 Modelling of Lumbar Cage

The whole 3D sketching of the lumbar cage implant is sketched using the SolidWorks software, and the whole process of sketching will be detailed in the following orders [4]. The sketching began by selecting the top view of the plane in the XY views and is followed by a 2D square sketching with a dimension of 32 mm in length and 12 mm in height. The sketching was then extruded to a 3D model by extruding it with a thickness of 28mm. These dimensions were referred from a previous study and a generalization assumption was done referring to previous research papers. The cuboidal spinal cage was selectively filleted on the 12 edges, with a curved dimension of 0.65 mm with a purpose of softer and less sharp corners and edges that do not disrupt the lumbar column once it has been placed into the human body. The diameter of the porous holes is 3 mm with uneven spacing between the holes whereas the height of the slots is kept constant at 6mm.

Figure 1 and 2 below shows the reference images for the porous holes and slots at the side surface of the cages, while the larger hole in the front surface is called the insertion that is used for the implementation to the surgical tool during the surgical process.

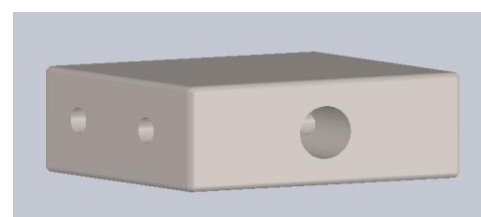


Fig.1. Spinal Cage with Holes

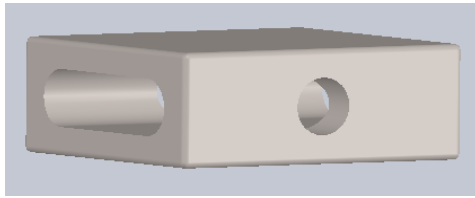


Fig.2. Spinal Cage with Slots

Table 1. Details of all 8 Specimens and the Number of Pores

Specimen	Number of Holes	Number of Slots
0	0	0
1	2	0
2	4	0
3	6	0
4	8	0
5	10	0
6	0	1
7	0	2

The volumes of all the cages would undoubtedly vary from one and another, thus the calculation of porosity percentage was implemented using the equation below:

$$\% \text{ of Porosity} = \frac{\text{Volume of Pores, mm}^3}{\text{Total Specimen Volume, mm}^3} \times 100\%$$

2.2 Material

The biomaterial implemented to all the spinal cages in ANSYS is annealed titanium alloy (annealed, Ti-6Al-4V)[1]. Since any additional heating element is added to a material that includes annealing, it thoroughly improves the particular material's strength and overall properties. The in-depth properties of the annealed titanium alloy are shown in the following table.

Table 2. Properties of Annealed Titanium Alloy

Properties	Values
Density, ρ	4429 kg/m ³
Young's Modulus, E	111.2 GPa
Poisson Ration, ν	0.3387
Ultimate Tensile Strength, UTS	918 MPa
Yield Strength	845.7 MPa
Isotropic Thermal Conductivity, k	7.187 W/m. °C

2.3 Finite Element Analysis (FEA)

Before proceeding with FEA, the specimens were validated using a mesh independency test with the variation in resolution. The highest available mesh resolution was 7, thus all specimens proceeded with

resolution 7. However, specimen 5 was not able to be meshed using the finest resolution as it attained topological edges meshing constraint.

The two required loadings that resemble the human body weight, as well as their respective motion, could be closest related to force and bending moment. These two loadings were applied on each spinal cage, in which the force applied was 1500 N whereas the moment was 1500 N.m. Both the loadings were applied on the top surface on the centre, while the bottom surface was selected as the fixed surface. The lumbar cage will be designed based on the findings of other authors, in which any sort of modification that needs to be done, will be simulated on a pre-existing model. Also, a few lumbar cages with different types of porosity will be examined, to study and understand the structural geometry with the mechanical properties or performance of the stress developed in the cage, under different loading conditions. The boundary conditions of the FEA will only be applied with a static preload and a right lateral bending moment to the cage. Mesh Independency Test (MIT) will also be used to validate the lumbar cage, in which the meshing quality such as aspect ratio, the skewness, and orthogonality quality and element quality will be used, and the sole purpose for this is to monitor or evaluate the accuracy of the FEA results[5]. Finally, the topological optimisation that is implemented in this study, limits to obtaining the specimen's design and does not proceed to analyse the final specimen on its stress analysis.

2.4 Topology Optimization

Table 3. ANSYS Settings

ANSYS Settings	Criteria	Values
Response Constraint	Mass	-
Percent to Retain	-	60 %
Number of Iterations	-	27

As shown in Table 3 and 4, the optimization was done in both software, ANSYS and SpaceClaim, in which it was a proceeding process after the static structural analysis. In ANSYS, two regions were required as part of the optimization, and they were the exclusion regions and design regions. The exclusion region will be the boundary condition by default, which is the top surface and bottom surface, whereas the design region were the regions to be optimized. Below is the parameter setup for the topology optimization in ANSYS and SpaceClaim.

Table 4. SpaceClaim Settings

SpaceClaim Settings	Criteria	Values
Shrink-wrap	Gap Size	5mm
Smooth Threshold Angle	-	360°
Smooth Features	i) Flatten Peaks ii) Volume Aware	-

3. RESULTS AND DISCUSSION

3.1 Porosity Analysis of Each Specimen

Porosity analysis allows us to obtain a better view of the overall structural properties in terms of the pore volume as well as its respective percentages when compared to the initial total volume. Despite specimen 0 being a control in which it only has one insertion hole, it is also being analysed to be compared with the other specimens that have a higher number of holes surrounding the specimens. The total volume of 10726.26 mm³ was obtained as a pure solid cuboidal shape excluding the insertion hole. Table 5 below shows the values obtained from the formula provided in the previous chapter, and the comparison of all 8 specimens after adding the insertion hole as well as the porous holes.

Table 5. Porosity Volume and Percentage for Each Specimen

Specimen	No of Holes	No of Slots	Total Volume (mm ³)	Pore Volume (mm ³)	Porosity (%)
0	0	0	10726.26	791.69	7.3809
1	2	0	10726.26	1162.65	10.8393
2	4	0	10726.26	1633.17	15.2259
3	6	0	10726.26	2031.02	18.9350
4	8	0	10726.26	2444.51	22.7900
5	10	0	10726.26	2930.63	27.3220
6	0	1	10726.26	4008.36	37.3696
7	0	2	10726.26	4299.83	40.0869

As we can see from the above table, the pore volume and the porosity percentage increased together in a steady-state from specimen 0 to 5. The percentage increase ranged anywhere from 3% to 5% between specimens 0 to 5. However, there was a spike in the porosity percentage between specimen 5 and 6, as the increase was approximately 10%, and this is mainly due to the number of holes on specimen 5 were 10 holes, and their

respective pore volume was only 2930.63mm³, yet the implementation of only 1 particular slot volume was tremendously larger than the total volume of 10 holes, as the volume of the slot for specimen 6 is 4008.36mm³ and specimen 7 having 2 slots has its pore volume of 4299.83mm³. Hence, it is clear to us that despite having either holes or slots, the porosity percentage increase is dependent on the volume of the pores and is independent of the number of holes or slots present in a particular specimen.

3.2 Mesh Independency Test

The results obtained for this test were varied between resolutions 1 to 7 on all specimens with their respective values. However, only the mesh metrics values of resolution 7 have proceeded for further analysis of this simulation. The table below shows the mesh metrics values of each specimen with resolution 7. Theoretically, a finer and higher resolution mesh produces a more accurate result for the analysis and solution, thus this supports the idea of proceeding with the analysis with the highest resolution that the software is capable of, and that is resolution 7. Furthermore, the higher resolution will produce a higher number of nodes and elements. Thus, improving the accuracy of the simulation. The specimen 5 is omitted in the simulation due to its inability to proceed with the meshing of resolution 7 due to the topological edges meshing constraint. Nonetheless, the analysis was still proceeded with all specimens implementing resolution 7, whereas specimen 5 alone is continued with resolution 5.

Table 6. (a) Mesh Independency Results with Resolution 7

Specimen	Number of Nodes	Number of Elements	Aspect Ratio
0	267166	132699	2.4749
1	350665	174563	2.3682
2	395639	196006	2.3058
3	459060	227142	2.202
4	505655	248620	2.1447
6	336339	166308	1.9889
7	368853	181833	1.9816

(b) Mesh Independency Results with Resolution 7

Specimen	Skewness	Element Quality	Orthogonal Quality
0	0.19773	0.18486	0.19416
1	0.20241	0.18507	0.19854
2	0.20774	0.20416	0.19196
3	0.20956	0.19465	0.20624
4	0.21255	0.20108	0.20918
6	0.205	0.18594	0.20168
7	0.20728	0.18879	0.20433

3.3 FEA Results

The simulated results of the finite element analysis were obtained from the ANSYS software, and all 8 specimens were evaluated separately on their reactions towards the structural analysis applied on each of them [6]. These 8 specimens were evaluated based on three surfaces, which are the top surface, middle lateral as well as the pores present. The graphs were plotted based on the porosity of each specimen instead of the names of their specimen for a more accurate reference purpose. This means that according to the porosity table in the previous subtopic, the specimens are arranged accordingly from 0 to 7 based on a reference to their respective porosity percentage. The results were further discussed on their reactions with comparisons of graphs and reference images for each surface. From these results, one specimen will be chosen for topological optimisation, which excludes the control specimen 0, and this will be further discussed in the following subtopics.

3.3.1 Stress Distribution on Top Surface

The top surface is considered an important surface to be analysed due to both the moment and force loadings are acting perpendicular to it. Thus the amount of stress this surface exerts needs to be discussed. The force and moment were applied exactly on the centre of the top surface to obtain more well-distributed stress on the overall specimens. The table below shows an overview for each specimen's stress distribution of Von Misses Stress and Maximum Principal Stress, and the blue and red tags on each picture represents the minimum and maximum stress exerted on the exact region.

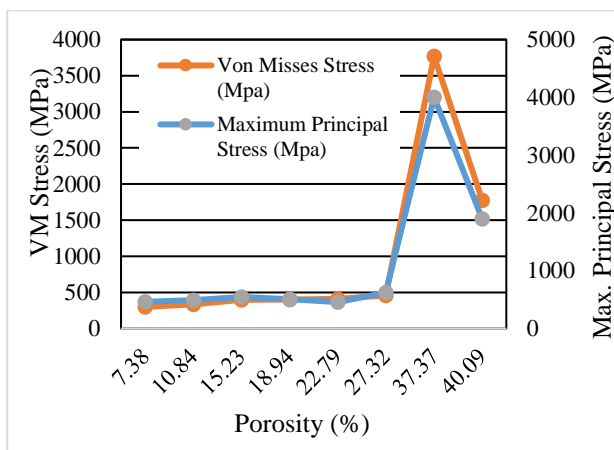


Fig. 3. Von Misses Stress and Maximum Principal Stress Against Porosity of Specimen

As shown in the graph, the change in trend for both the Von Misses Stress and Maximum Principal Stress are approximately identical as their values of inclination and declination were occurring on the same specimens. The highest value or rather the biggest jump of data in both stresses occurred on specimen 6, with the porosity of 37.37%. It was due to the volume of pores dispersed around the specimen were different compared to the typical hole's arrangement. Despite the holes having an increase in the percentage value, there was still a certain solid fill between each hole, whereas, for slots, it was an open solid cut, thus the stress acted highly on specimen 6, which then later dropped back slightly on specimen 7, due to similar solid fill when another slot was added. For

this surface, specimen 1 has obtained the least amount of stress concentration when the loadings were applied.

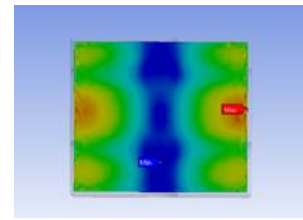


Fig. 4. Specimen 1 Von Misses Stress

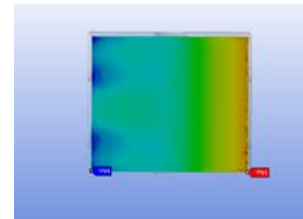


Fig. 5. Specimen 1 Maximum Principal Stress

3.3.2 Stress Distribution on Middle Lateral

For the middle lateral surface, the analysis was done by the implementation of section planes, in which the overall specimens' stresses were observed, then followed by sectioning the specimens into halves. This enabled the results of the stress and the position of maximum and minimum regions to be observed more clearly in the internal surface. Below is the image overview of the stresses concentrations on the middle lateral.

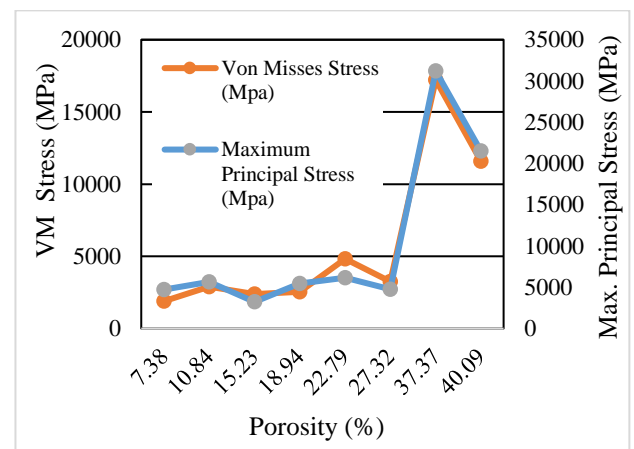


Fig. 6. Von Misses Stress and Maximum Principal Stress Against Porosity of Specimen

For the middle lateral surface, the stresses values were not as identical as the top surface as there were variations of high and low on different specimens. There was a small jump in Von Misses Stress value in specimen 4 before slightly dropping back on specimen 5. However, the major escalation occurred on specimen 6 as well, and this is mainly due to the arrangement or placement of the slots in the specimen as the slot was extruded in the centre of the specimen as a whole hollow. Thus the stress exerted were roughly the same as the top surface. On the other hand, specimen 2 with a porosity of 15.23% obtained the lowest Maximum Principal Stress when compared to the other specimens, and obtained the lowest Von Misses Stress when the control specimen with a porosity of 7.38% is neglected. The explanation to aid this result comes down to this specimen had the first

arrangement of double-layer holes, 2 holes on the first layer and 2 holes on the second layer, thus exerting lower stress as the middle cross-section has a sectioned pore, when compared to the other specimens. This shows that the middle section of this specimen exerted low stress due to the presence of the sectioned pores. For the middle lateral surface, specimen 2 was favoured as having the least stress concentration compared to the other specimens.

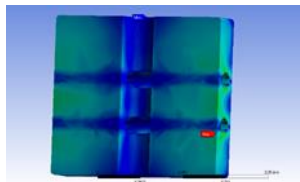


Fig.7. Specimen 2 Von Misses Stress

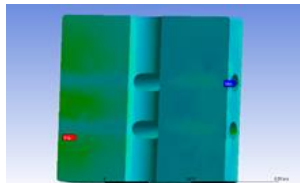


Fig. 8. Specimen 2 Maximum Principal Stress

3.3.3 Stress on Pores

The final region to be analysed on the FEA results was the stresses on the pores, which includes the insertion hole as well. The stresses of pores were obtained by implementing the “highlight” feature in ANSYS which enabled the selection of only the porous holes or slots without sectioning or selecting a surface to proceed with the evaluation.

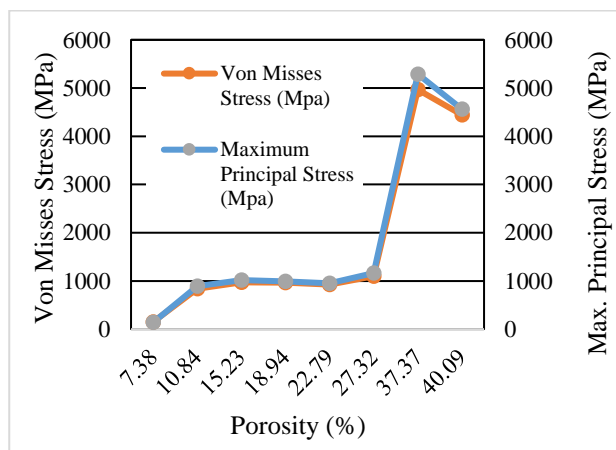


Fig. 9. Von Misses Stress and Maximum Principal Stress Against Porosity of Specimen

From the figure, both stresses exerted on the pores of all 8 specimens had a steady inclination as the porosity of the specimens increased until it reached specimen 5. A huge escalation of approximately 4000 MPa for Von Misses Stress and approximately 4100 MPa for Maximum Principal Stress occurred from specimen 5 to 6 and this is due to arrangement and the hollow gap of the slot in specimen 6. When a huge load of 1500 N was applied, the pores will be one of the main regions to

experience the highest stress, as it is being compressed by the top surface bending into the pores. Specimen 1 obtained the lowest stress exertion when compared to other specimens, thus it is clear that specimen 1 is more favourable to be chosen for further analysis of topology optimisation due to it being more dominant than specimen 2 as specimen 2 only had a low-stress concentration on one surface whereas specimen 1 had two surface dominance.

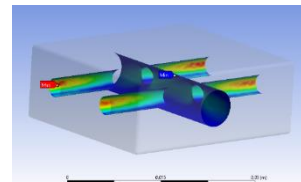


Fig. 9. Specimen 1 Von Misses Stress

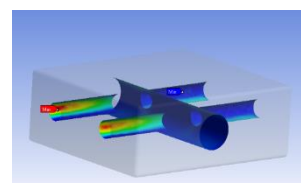


Fig. 10. Specimen 1 Maximum Principal Stress

3.4 Topology Optimization

Despite specimen 1 having more dominance in the low-stress exertion on 2 surfaces, it was also important to observe or evaluate the specimens in terms of fusion rate with the human body, which requires bone graft to be implemented in the spinal cage. Since specimen 1 has only 2 porous holes, the bone graft filling is limited to a certain volume filling whereas specimen 2 has more porous holes thus enabling more filling of the bone graft. This also shows that specimen 2 was the most favoured as it completed the overall requirement to be able to maintain stable stress concentration while performing inside the human body.

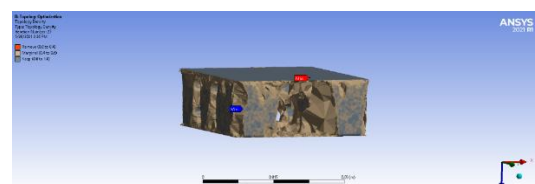


Fig. 11. Post-Topological Optimisation Shape Overview

Fig. 11 shows the image of specimen 2 after undergoing the topological optimisation process, in which it has removed most of its material from the specimen to obtain its most optimal shape for a given design of space whilst having the loads acting on it. This method allowed minimum volume of material while maintaining the structural strength. The shape of the optimized cage has slightly lost its original cuboidal shape with mainly the insertion hole and the edges of the specimen having rough and distorted surfaces. As the purpose of this process is to obtain a lightweight specimen for manufacturing and to cut down development costs, it was necessary to proclaim the end product after removing a

certain amount of mass and volume, without actually affecting the performance of the product. This is because any model that has undergone topological optimisation has proven to obtain the most amount of material required to be used in which the stresses are exerting only on those regions, thus removing the unnecessary materials, hence the reduction in overall mass and volume. A feature that needed to be emphasized was the comparison of initial mass and volume with the results of post optimisation, and the comparison is as shown below.

Table 6. Comparison of Mass and Volume of Specimen of Pre and Post Optimisation

Parameters	Pre-Optimisation	Post-Optimisation
Mass (kg)	0.040273	0.026426
Volume (m ³)	0.000009093	0.000005966

For both parameters, the specimen's removal percentage of material was 34.38% from the original specimen, therefore this has shown that quite an amount of material itself has been removed for the optimum end product to be finalised. Previous studies stated that the removal percentage was ranging anywhere from 30% to 50%, thus this could be generalized that the current studied material's removal percentage was within the tolerance range[7]. However, the end product post-optimisation did not have smooth edges as mentioned above, thus SpaceClaim was used to complete the smoothening process of the specimen, for it to be presentable to initiate a new development of a product. Surface finishing was done on every part of the specimen such as peaks flattening to remove sharp edges and peaks that could distort the stress concentration when it is implemented in the actual human spine. Below are the top and side view figures of the completed surface finishing specimen.

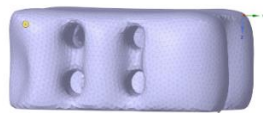


Fig. 12. Side View of the Optimised Spinal Cage

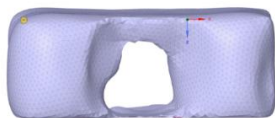


Fig. 13. Front View of the Optimised Spinal Cage

Despite the looks of the end product having a bulky outer characteristic, it can also be said as having rather smoother or more filled surfaces that cleared out all the sharp edges. This end product would require further assessment such as the static structural analysis on this model, to evaluate the stress concentration overview, however, this study limited its findings towards obtaining the best product to be marketed in terms of looks as of now and further analysis will be conducted for the proceeding requirements in the future.

4. CONCLUSION

To summarise, the topic of study was rather focused on design and research development on the spinal cage designs with the porosity volume analysis, implementing the titanium alloy material. A total of 8 specimens were designed which includes the controlled specimen as well, were designed and analysed via FEA to obtain its microstructural properties and the purpose is to be able to simulate the loading conditions such as force and moment on all the specimens. Thus, this shows that the first objective was achieved and the values for all 8 specimens have been detailed out on different tests that include mesh independency test, stress concentrations on different surfaces, and the porosity analysis.

Once the specimens have completed the FEA analysis, the confusion occurred on choosing one specimen to undergo topology optimisation, as theoretically it is known that a lower stress concentration specimen (lesser holes) was substantially optimal to be chosen for the following process. Specimen 2 is chosen and further optimised topologically to obtain the marketable product overview that would still require further modifications, yet achieving the objective of being able to obtain the best specimen for its respective purposes.

For future recommendations, it would be valuable to have insight from a comparative study using experiments.

5. ACKNOWLEDGEMENT

The authors would like to thanks the Universiti Malaysia Pahang (www.ump.edu.my) and Malaysia Ministry of Education, for laboratory facilities and financial assistance under FRGS-RACER Research Grant project No. RACER/1/2019/TK03/UMP//2.

6. REFERENCES

- [1] P. J. Rao, M. H. Pelletier, W. R. Walsh, and R. J. Mobbs, "Spine Interbody Implants: Material Selection and Modification, Functionalization and Bioactivation of Surfaces to Improve Osseointegration," *Orthop. Surg.*, vol. 6, no. 2, pp. 81–89, 2014.
- [2] P. I. J. M. Wuisman and T. H. Smit, "Bioresorbable polymers: Heading for a new generation of spinal cages," *Eur. Spine J.*, vol. 15, no. 2, pp. 133–148, 2006.
- [3] M. H. Jalil, M. H. Mazlan, and M. Todo, "Biomechanical Comparison of Polymeric Spinal Cages Using Ct Based Finite Element Method," *Int. J. Biosci. Biochem. Bioinforma.*, vol. 7, no. 2, pp. 110–117, 2017.
- [4] S. Hisyam and T. Mitsugu, "Biomechanical Analysis of Hypertrophic Cardiomyopathy Behavior of Human Heart using Dynamic Finite Element Method," in *Proceeding of International Exchange and Innovation Conference on Engineering & Sciences (IEICES) 5*, 2019, pp. 60–62.
- [5] M. Lee, G. Park, C. Park, and C. Kim, "Improvement of Grid Independence Test for Computational Fluid Dynamics Model of Building Based on Grid Resolution," *Adv. Civ. Eng.*, vol. 2020, 2020.
- [6] W. F. Wan Fatimatul Aifaa, M. Mohammad Azeeb, H. Fazah Akhtar, and A. Abdul Halim, "Development of 3D Printed Socket for Transtibial Prosthetic Leg,"

in *Proceeding of International Exchange and Innovation Conference on Engineering & Sciences (IEICES)* 5, 2019, pp. 44–46.

- [7] H. Kang, S. J. Hollister, F. La Marca, P. Park, and C.-Y. Lin, “Porous Biodegradable Lumbar Interbody Fusion Cage Design and Fabrication Using Integrated Global-Local Topology Optimization With Laser Sintering,” *J. Biomech. Eng.*, 2013.